

Effective Field Theory for Atom-Molecule Systems II: Stationary Solutions and Bogoliubov Excitations in Atom-Molecule Systems

Catarina E Sahlberg and C W Gardiner

*Jack Dodd Centre for Quantum Technology,
Department of Physics, University of Otago,
Dunedin, New Zealand*

October 10, 2018

Abstract

We formulate the basic theoretical methods for Bose–Einstein condensation of atoms close to a Feshbach resonance, in which the tunable scattering length of the atoms is described using a system of coupled atom and molecule fields. These include the Thomas–Fermi description of the condensate profile, the c-field equations, and the Bogoliubov–de Gennes equations, and the Bogoliubov excitation spectrum for a homogenous condensed system. We apply this formalism to the special case of Bragg scattering from a uniform condensate, and find that for moderate and large scattering lengths, there is a dramatic difference in the shift of the peak of the Bragg spectra, compared to that based on a structureless atom model. The result is compatible with the experimental results of [1].

1 Introduction

A recent experiment on Bragg scattering of a Bose-Einstein condensate (BEC) close to a Feshbach resonance [1], investigated the effect of varying the interatomic scattering length on the position of the Bragg spectral peak. This experiment used values of scattering length, much larger than have previously been used in Bragg scattering experiments, and noted that there was no theoretically justifiable method of describing a BEC in this regime.

In *Paper I* [2] we formulated a method for treating ultracold atoms close to a Feshbach resonance as a system of coupled atom and molecule fields. This method is applicable in the regime covered by the experiment, and has been developed in such a way as to be directly applicable to a c-field description of a BEC in the vicinity of a Feshbach resonance. The aim of this paper is to formulate the standard results, such as the Thomas–Fermi profiles and the Bogoliubov spectrum, appropriate to this model of systems of condensed atoms and molecules, and describe the differences which arise compared to the corresponding theories of structureless atoms with the same scattering length.

This paper is a precursor to our next paper, in which full c-field computations of Bragg scattering will be performed, in a way which is directly comparable with the experiment of [1]. Here, we apply this model to the case of ideal Bragg scattering from a uniform condensate, and compare this with the corresponding theory for a BEC of

structureless atoms, as done previously in [3]. By doing this we obtain a benchmark comparison of the behaviour of a Feshbach molecule treatment with that of the structureless atom models, avoiding the numerous complexities which necessarily arise in experiments. Thus, we can isolate the effects which arise *only* from the dynamics of the molecular basis of the Feshbach resonance, from those which are forced on us by the practicalities of experimental procedure.

2 Formalism

The formalism used here is outlined in *Paper I* [2] and is based on the c-field methods described in detail in [4].

2.1 Phenomenological Hamiltonian for atom-molecule system

As introduced in *Paper I*, the Hamiltonian of a coupled atom-molecule system is given by

$$\hat{H} = \int dx \left\{ \hat{\psi}^\dagger(\mathbf{x}) \left(-\frac{\hbar^2 \nabla^2}{2m} + V_a(\mathbf{x}) \right) \hat{\psi}(\mathbf{x}) + \hat{\phi}^\dagger(\mathbf{x}) \left(-\frac{\hbar^2 \nabla^2}{4m} + V_m(\mathbf{x}) + \varepsilon \right) \hat{\phi}(\mathbf{x}) + \frac{U_{aa}}{2} \hat{\psi}^\dagger(\mathbf{x}) \hat{\psi}^\dagger(\mathbf{x}) \hat{\psi}(\mathbf{x}) \hat{\psi}(\mathbf{x}) + U_{am} \hat{\psi}^\dagger(\mathbf{x}) \hat{\phi}^\dagger(\mathbf{x}) \hat{\phi}(\mathbf{x}) \hat{\psi}(\mathbf{x}) + \frac{U_{mm}}{2} \hat{\phi}^\dagger(\mathbf{x}) \hat{\phi}^\dagger(\mathbf{x}) \hat{\phi}(\mathbf{x}) \hat{\phi}(\mathbf{x}) + \frac{g}{2} \left(\hat{\phi}^\dagger(\mathbf{x}) \hat{\psi}(\mathbf{x}) \hat{\psi}(\mathbf{x}) + \hat{\psi}^\dagger(\mathbf{x}) \hat{\psi}^\dagger(\mathbf{x}) \hat{\phi}(\mathbf{x}) \right) \right\}, \quad (1)$$

where $U_{aa} = 4\pi\hbar^2 a_{bg}/m$ is the background interaction strength and V_a and V_m are the external trapping potential for the atoms and molecules respectively. The terms with factors U_{am} and U_{mm} correspond to atom-molecule and molecule-molecule scattering. However, in the systems considered here, the molecule field arises only during collisions, and is very small, making these terms negligible.

2.1.1 Values of parameters

The parameters g and ε are the coupling strength and detuning in the Feshbach resonance respectively. In our formalism they are given in terms of the experimentally measurable binding energy and s-wave scattering length by

$$\varepsilon = \frac{\hbar^2 \alpha^2 (\pi - 2\Lambda a_s) \left(1 - 2\Lambda a_{bg} t(\frac{\alpha}{\Lambda}) / \pi \right)}{2m \Lambda a_s (1 + t(\frac{\alpha}{\Lambda})) - \pi}, \quad (2)$$

$$g^2 = \frac{8\pi\hbar^4 \alpha^2 (a_{bg}(\pi - 2\Lambda a_s) - \pi a_s) \left(1 - 2\Lambda a_{bg} t(\frac{\alpha}{\Lambda}) / \pi \right)}{m^2 2\Lambda a_s (1 + t(\frac{\alpha}{\Lambda})) - \pi}. \quad (3)$$

where $t(x) = x - \arctan 1/x$, the parameter Λ is the momentum space cutoff, and $\hbar^2 \alpha^2 / m$ is the molecule binding energy for a certain value of the s-wave scattering length a_s [2]. It is important to note that in this phenomenological model the parameters ε and g take on different values, depending on the closeness to the Feshbach resonance.

In this paper we will consider a BEC of ^{85}Rb , for which there is experimental data of the binding energy close to the Feshbach resonance at 155 G [5]. For a given momentum cutoff Λ we can then calculate the values of the coupling g , and detuning ε , for each value of the scattering length, using equations (3) and (2). We fit curves to the values calculated from the experimental data in order to extrapolate to other values of the scattering length. The data, obtained using (2) and (3) are well fitted by a linear relationship

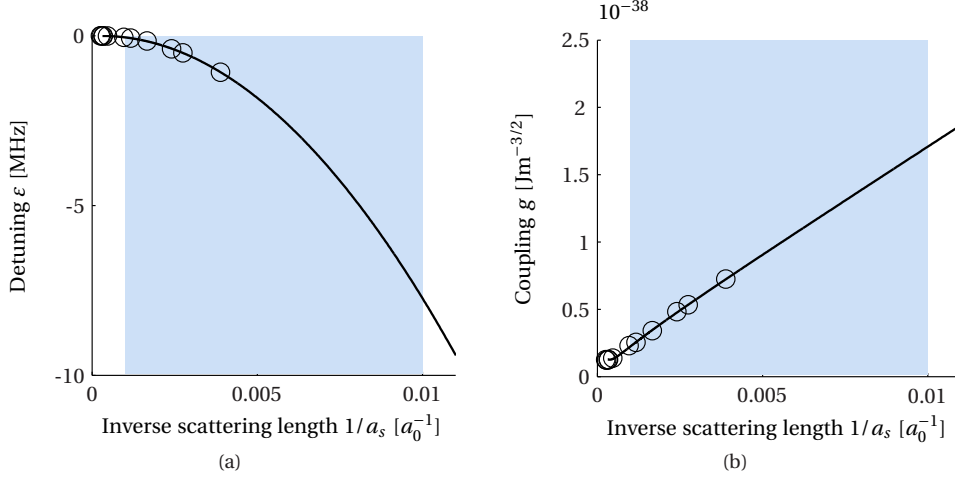


Figure 1: The Feshbach resonance detuning ε , and coupling parameter g , as functions of the inverse scattering length. The black circles indicate the values calculated using the experimental data from [5] and equations (3) and (2). The black lines are fits to these calculated values. The shaded blue areas indicate the range of scattering lengths of interest in the experiment of [1], as well as in the later sections of this paper. The momentum cutoff is here chosen to be $\Lambda = 10^6 \text{ m}^{-1}$.

between g and a_s^{-1} , and a quadratic relationship between ε and a_s^{-1} . We show the data and fits in Fig. 1.

2.1.2 C-field equations

Since the atom field is usually much larger than the molecule field in the situations we shall consider, we can set U_{am} and U_{mm} equal to zero and the c-field equations of motion corresponding to the Hamiltonian (1) become

$$i\hbar \frac{\partial \psi(\mathbf{x})}{\partial t} = \left(-\frac{\hbar^2 \nabla^2}{2m} + V_a(\mathbf{x}) \right) \psi(\mathbf{x}) + U_{aa} |\psi(\mathbf{x})|^2 \psi(\mathbf{x}) + g \psi(\mathbf{x})^* \phi(\mathbf{x}), \quad (4)$$

$$i\hbar \frac{\partial \phi(\mathbf{x})}{\partial t} = \left(-\frac{\hbar^2 \nabla^2}{4m} + \varepsilon + V_m(\mathbf{x}) \right) \phi(\mathbf{x}) + \frac{g}{2} \psi^2(\mathbf{x}). \quad (5)$$

In practice, when solving these equations numerically, it is necessary to explicitly use a projector in order to restrict the wavefunctions to the momentum subspace below the cutoff Λ , as described in *Paper I* and implemented in *Paper III*.

The value of the momentum space cutoff Λ will, in the case of numerical simulation, arise from the simulation grid; any such computation is restricted to a finite number of momentum space modes. It is also necessary to introduce a projector in order to avoid effects from aliasing [4]. Furthermore, a momentum cutoff is necessary in order for the pseudopotential approximation to be valid [6]. However, as we show in *Paper I*, the actual choice of value for the cutoff required for our simulations has only a very small effect on the values of the phenomenological Hamiltonian parameters.

2.2 Thomas-Fermi Solutions

Stationary solutions to the equations of motion (4) and (5) can be obtained by letting the time evolution of the wavefunctions be $\psi(\mathbf{x}, t) = \psi(\mathbf{x}) \exp(i\mu_a t/\hbar)$ and $\phi(\mathbf{x}, t) = \phi(\mathbf{x}) \exp(i\mu_m t/\hbar)$.

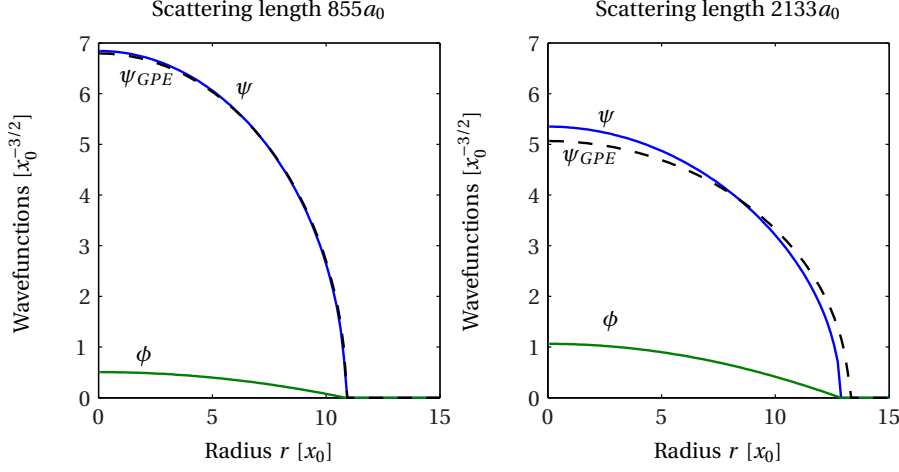


Figure 2: Thomas-Fermi profiles for a spherically symmetric condensate of ^{85}Rb for two of the different scattering lengths reported in Ref. [5]: $a_s = 856a_0$ (left panel) and $a_s = 2133a_0$ (right panel). The trapping frequency is $\omega_x = 2\pi \times 17.5$ Hz, and the total particle number — counting each molecule as two atoms — is 10^5 . The blue solid lines are the atom Thomas-Fermi profiles from (8), the green solid lines are the molecule profiles given by (9), and the dashed black lines are the Thomas-Fermi profiles obtained from the Gross-Pitaevskii equation. The parameter x_0 is the length scale associated with the trap, given by $x_0 = \sqrt{\hbar/2m\omega_x}$.

It is clear that $\mu_m = 2\mu_a$ in order for the coupling terms to be time-independent, so we get

$$\mu_a \psi(\mathbf{x}) = \left(-\frac{\hbar^2 \nabla^2}{2m} + V_a(\mathbf{x}) \right) \psi(\mathbf{x}) + U_{aa} |\psi(\mathbf{x})|^2 \psi(\mathbf{x}) + g \psi(\mathbf{x})^* \phi(\mathbf{x}), \quad (6)$$

$$2\mu_a \phi(\mathbf{x}) = \left(-\frac{\hbar^2 \nabla^2}{4m} + \varepsilon + V_m(\mathbf{x}) \right) \phi(\mathbf{x}) + \frac{g}{2} \psi(\mathbf{x})^2. \quad (7)$$

Taking the Thomas-Fermi limit and solving for ψ and ϕ gives the Thomas-Fermi solutions

$$|\psi_s(\mathbf{x})| = \sqrt{\frac{\mu_a - V_a(\mathbf{x})}{U_{aa} + g^2/2(2\mu_a - \varepsilon - V_m(\mathbf{x}))}}, \quad (8)$$

$$\phi_s(\mathbf{x}) = \frac{g}{2(2\mu_a - \varepsilon - V_m(\mathbf{x}))} \psi^2(\mathbf{x}). \quad (9)$$

Fig. 2 shows the Thomas-Fermi wavefunctions for a spherically symmetric condensate of 10^5 atoms of ^{85}Rb . The Thomas-Fermi solution for the atom wavefunction is similar to that for the structureless model for the same atom number and scattering length (also shown in the figure), with the important difference that the denominator has a spatial dependence. As long as the scattering length is moderate (left panel of figure 2), the detuning ε will be large and the molecular trapping potential will be negligible in comparison, making the Thomas-Fermi solution indistinguishable from the standard Thomas-Fermi solution. However, for very large scattering lengths (right panel of figure 2), the detuning ε will be small enough for the molecular trapping potential to be significant, making the atom-molecule Thomas-Fermi profile different from that of the structureless atom model.

Also, note that in (8), since the potential $V_m(\mathbf{x})$ is normally negligible compared to $2\mu_a - \varepsilon$, the Thomas-Fermi solution for the atomic field is essentially of the same form

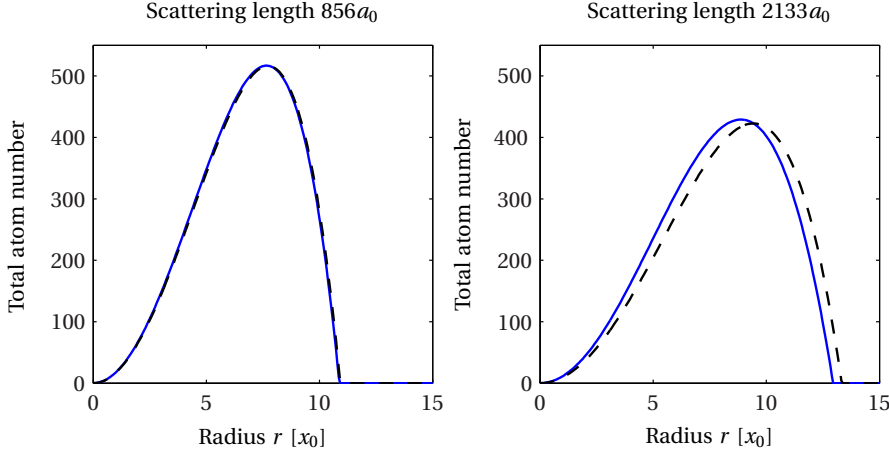


Figure 3: Density for a spherically symmetric condensate of ^{85}Rb for two of the different scattering lengths reported in Ref. [5]: $a_s = 856a_0$ (left panel) and $a_s = 2133a_0$ (right panel). The system is the same as that in figure 2. For this system, the portion of atoms in the form of molecules is approximately 0.6% for $a_s = 856a_0$ and 4.5% for $a_s = 2133a_0$. (Note: At first glance, it appears that the solution ψ_{GPE} has fewer atoms, than given by the atom-molecule model, but, as can be seen in the right hand figure, the discrepancy in the centre is compensated by at the wings, where the extra factor of $4\pi r^2$ becomes more significant.)

as that for the GPE at the same chemical potential. However, for the same total number of atoms — counting each molecule as two atoms — the chemical potential for the GPE is slightly different from that found in this model. As well as this, the molecule field corresponds to the number of *elementary* molecules, and each *physical molecule* is a superposition of an elementary molecule and an atom pair, as discussed in *Paper I*. Closer to the Feshbach resonance, the proportion of atom pairs can become more than 50%, although in the systems we study here, these effects will be so small that they can be neglected.

The atom density of the condensate in the Thomas-Fermi limit is given by

$$n(\mathbf{x}) = |\psi_s(\mathbf{x})|^2 + 2|\phi_s(\mathbf{x})|^2. \quad (10)$$

Fig. 3 shows the density profile for a spherically symmetric condensate of 10^5 atoms of ^{85}Rb in the Thomas-Fermi limit. For comparison we have also plotted the Thomas-Fermi density profile obtained from a structureless atom model for the same scattering length and atom number.

3 Quasiparticle excitations

In the Bogoliubov approximation, the field operator can be separated into a mean-field ground state and an operator part describing the excitations. In our coupled system, we expand the atom and molecule wavefunctions in terms of quasiparticle bases as

$$\begin{pmatrix} \psi(\mathbf{x}, t) \\ \phi(\mathbf{x}, t) \end{pmatrix} = \begin{pmatrix} \psi_0(\mathbf{x}) \\ \phi_0(\mathbf{x}) \end{pmatrix} + \sum_p \left\{ \begin{pmatrix} u_p(\mathbf{x}) \\ r_p(\mathbf{x}) \end{pmatrix} \hat{b}_p e^{-i\omega_p t} + \begin{pmatrix} v_p^*(\mathbf{x}) \\ s_p^*(\mathbf{x}) \end{pmatrix} \hat{b}_p^\dagger e^{i\omega_p t} \right\}, \quad (11)$$

where the first terms are the condensate atom and molecule ground state wavefunctions, and \hat{b}_p and \hat{b}_p^\dagger are the quasiparticle destruction and creation operators respectively. Unlike the standard Bogoliubov expansion, where the only mixture is between the atom

creation and destruction terms, in this case it is also necessary to include the molecule creation and destruction terms. The quasiparticle operators in this expansion thus have both atom and molecule components.

3.1 Two-component Bogoliubov-de Gennes equations

Making these substitutions to the equations of motion (4) and (5) gives, after collecting terms with the same phase, the two-component Bogoliubov-de Gennes equations

$$\mathcal{L}\mathbf{U}_p + \mathcal{M}\mathbf{V}_p = \hbar\omega_p\mathbf{U}_p, \quad (12)$$

$$\mathcal{L}\mathbf{V}_p + \mathcal{M}^\dagger\mathbf{U}_p = -\hbar\omega_p\mathbf{V}_p, \quad (13)$$

where $\mathbf{U}_p = (u_p(\mathbf{x}), r_p(\mathbf{x}))^T$ and $\mathbf{V}_p = (v_p(\mathbf{x}), s_p(\mathbf{x}))^T$. Here \mathcal{L} is Hermitian, but \mathcal{M} need not be Hermitian. In our case they are given by

$$\mathcal{L} = \begin{pmatrix} -\frac{\hbar^2\nabla^2}{2m} + V_a(\mathbf{x}) - \mu_a + 2U_{aa}\psi_0(\mathbf{x})^2 & g\psi_0(\mathbf{x}) \\ g\psi_0^*(\mathbf{x}) & -\frac{\hbar^2\nabla^2}{4m} + \varepsilon + V_m(\mathbf{x}) - 2\mu_a \end{pmatrix}, \quad (14)$$

$$\mathcal{M} = \begin{pmatrix} U_{aa}\psi_0(\mathbf{x})^2 + g\phi_0(\mathbf{x}) & 0 \\ 0 & 0 \end{pmatrix}. \quad (15)$$

Both \mathcal{L} and \mathcal{M} are in fact Hermitian. When ψ_0 and ϕ_0 are chosen to be real, they are also symmetric. The multi-component equations (12, 13) are similar to the single-component ones. Indeed, if we let $g \rightarrow 0$ in these equations, the upper components obey the standard Bogoliubov-de Gennes equation for a single atom field.

3.2 Orthogonality and normalisation conditions

The normalisation and orthogonality conditions of the quasiparticle amplitudes can be derived by using the symmetry properties of \mathcal{L} and \mathcal{M} , for details see the appendix. We get the conditions

$$\int d\mathbf{x} (\mathbf{U}_{p'}^\dagger \mathbf{U}_p - \mathbf{V}_{p'}^\dagger \mathbf{V}_p) = \delta_{p,p'}, \quad (16)$$

$$\int d\mathbf{x} (\mathbf{V}_p^T \mathbf{U}_{p'} - \mathbf{U}_p^T \mathbf{V}_{p'}) = 0. \quad (17)$$

We can also use the Bose commutation relations for the components of $\boldsymbol{\psi} = (\psi, \phi)^T$,

$$[\boldsymbol{\psi}_\alpha(\mathbf{x}), \boldsymbol{\psi}_\beta^\dagger(\mathbf{x}')] = \delta_{\alpha,\beta}\delta(\mathbf{x} - \mathbf{x}'), \quad (18)$$

$$[\boldsymbol{\psi}_\alpha(\mathbf{x}), \boldsymbol{\psi}_\beta(\mathbf{x}')] = 0, \quad (19)$$

from which we get the conditions

$$\sum_p (\mathbf{U}_{\alpha,p} \mathbf{U}_{\beta,p}^* - \mathbf{V}_{\alpha,p}^* \mathbf{V}_{\beta,p}) = \delta_{\alpha,\beta} \quad (20)$$

$$\sum_p (\mathbf{U}_{\alpha,p} \mathbf{V}_{\beta,p}^* - \mathbf{V}_{\alpha,p}^* \mathbf{U}_{\beta,p}) = 0. \quad (21)$$

The four conditions (16, 17, 20, 21) are related; indeed (20) and (21) can be derived from (16) and (17).

4 Uniform condensate

If considering a uniform condensate, the Thomas-Fermi solutions (8, 9) are exact and give

$$\psi_0 = \sqrt{\frac{\mu_a}{U_{aa} + g^2/2(2\mu_a - \varepsilon)}} \equiv \sqrt{n_a}, \quad (22)$$

$$\phi_0 = \frac{g}{2(2\mu_a - \varepsilon)} \psi^2 \equiv \sqrt{n_m}, \quad (23)$$

where we have chosen ψ_0 to be real and positive.

For the uniform condensate, the quasiparticle amplitudes can be expressed as plane waves, according to

$$u_{k,l}(\mathbf{x}) \rightarrow \frac{u_{k,l} e^{i\mathbf{k}\cdot\mathbf{x}}}{\sqrt{\mathcal{V}}} \quad (24)$$

$$v_{k,l}^*(\mathbf{x}) \rightarrow \frac{v_{k,l}^* e^{-i\mathbf{k}\cdot\mathbf{x}}}{\sqrt{\mathcal{V}}} \quad (25)$$

$$r_{k,l}(\mathbf{x}) \rightarrow \frac{r_{k,l} e^{i\mathbf{k}\cdot\mathbf{x}}}{\sqrt{\mathcal{V}}} \quad (26)$$

$$s_{k,l}^*(\mathbf{x}) \rightarrow \frac{r_{k,l}^* e^{-i\mathbf{k}\cdot\mathbf{x}}}{\sqrt{\mathcal{V}}}, \quad (27)$$

where \mathcal{V} is the volume of the system.

In this case we can express \mathcal{L} and \mathcal{M} as

$$\mathcal{L} = \begin{pmatrix} \frac{\hbar^2 k^2}{2m} - \mu_a + 2U_{aa}n_a & g\sqrt{n_a} \\ g\sqrt{n_a} & \frac{\hbar^2 k^2}{4m} + \varepsilon - 2\mu_a \end{pmatrix}, \quad (28)$$

$$\mathcal{M} = \begin{pmatrix} U_{aa}n_a + g\sqrt{n_m} & 0 \\ 0 & 0 \end{pmatrix}. \quad (29)$$

Since there will be two distinct eigenfrequencies for each value of the momentum \mathbf{k} — one corresponding to a state which is mainly atomic, and one corresponding to a state which is mainly molecular, as we shall see in the following section — the subscript p refers to the different momentum modes \mathbf{k} , as well as the two eigenvalues, which we refer to as the “atomic” ω_A and “molecular” ω_M . This terminology corresponds to the behaviour of the eigenvectors for sufficiently small $|\mathbf{k}|$. The situation becomes somewhat complicated at higher values of $|\mathbf{k}|$, as we shall show in the next section.

4.1 Eigenvalues of the Bogoliubov-de Gennes equations

The eigenvalues of the Bogoliubov-de Gennes equations are now given explicitly by a somewhat intricate procedure as follows:

A : Define the quantities

$$\mathcal{R} \equiv \mathcal{L}_{11}^2 - \mathcal{M}_{11}^2 + \mathcal{L}_{22}^2, \quad (30)$$

$$\mathcal{S} \equiv (\mathcal{L}_{11}^2 - \mathcal{M}_{11}^2 - \mathcal{L}_{22}^2)^2 + 4\mathcal{L}_{12}^2 ((\mathcal{L}_{11} + \mathcal{L}_{22})^2 - \mathcal{M}_{11}^2). \quad (31)$$

B : define the quantities K^l and K^h as the smallest and largest positive values of $|\mathbf{k}|$ for which $\mathcal{S} = 0$.

C : For the range of values of $|\mathbf{k}|$ given by $0 \leq |\mathbf{k}| \leq K^l$,

$$\omega_{k,A} = \frac{1}{\sqrt{2}} \sqrt{\mathcal{R} - \sqrt{\mathcal{S}}}, \quad (32)$$

$$\omega_{k,M} = -\frac{1}{\sqrt{2}} \sqrt{\mathcal{R} + \sqrt{\mathcal{S}}}. \quad (33)$$

D : For the range of values of $|\mathbf{k}|$ given by $K^l \leq |\mathbf{k}| \leq K^h$,

$$\omega_{k,A} = \frac{1}{\sqrt{2}} \sqrt{\mathcal{R} - i\sqrt{|\mathcal{S}|}}, \quad (34)$$

$$\omega_{k,M} = -\frac{1}{\sqrt{2}} \sqrt{\mathcal{R} + i\sqrt{|\mathcal{S}|}}. \quad (35)$$

E : For the range of values of $|\mathbf{k}|$ given by $K^h \leq |\mathbf{k}|$,

$$\omega_{k,A} = \frac{1}{\sqrt{2}} \sqrt{\mathcal{R} + \sqrt{\mathcal{S}}}, \quad (36)$$

$$\omega_{k,M} = -\frac{1}{\sqrt{2}} \sqrt{\mathcal{R} - \sqrt{\mathcal{S}}}. \quad (37)$$

Fig. 4 shows the eigenvalues calculated using this procedure for a uniform condensate of ^{85}Rb with a total density of $n \equiv n_a + 2n_m = 10^{20} \text{ m}^{-3}$ at a scattering length of $900a_0$. Here we use the experimental values of the binding energy taken from [5] to determine ε and g , using Equations (2) and (3). The momentum is measured in units of the momentum q of the Bragg pulse in the experiment of Ref. [1] with $q = 1.6 \times 10^7 \text{ m}^{-1}$. The following points should be noted:

1. As can be seen clearly in the figure, the atomic eigenvalue $\omega_{k,A}$ is similar to that obtained from the Gross-Pitaevskii equation, but is slightly shifted from this, due to the coupling between the atoms and the molecules. This shift is not dramatic, but is still measurable, for example by using Bragg scattering, as in the experiment of [1].
2. The atomic eigenvalue $\omega_{k,A}$ belongs to the atom-dominated state. The energy to create an atom-dominated quasiparticle is thus $\hbar\omega_{k,A}$.
3. Similarly, the energy to create an molecule-dominated quasiparticle is given by $\hbar\omega_{k,M}$. Since $\omega_{k,M}$ is related to the binding energy of the molecules, and ε is negative, $\omega_{k,M}$ is also negative. Thus, the energy to create a molecule-dominated quasiparticle is *negative*, and increases with $|\mathbf{k}|$, which is expected for a bound state.
4. The higher eigenvalue $\omega_{k,M}$ has the same general behaviour as $\omega_{k,A}$, but since it is related to the binding energy of the molecules, it is shifted downwards. As $k \rightarrow 0$, and as long as the density is moderate, $\omega_{k,M}$ can be approximated by

$$\hbar\omega_{0,H} \approx \varepsilon + 2U_{aa}n - 4\mu_a, \quad (38)$$

and as $n \rightarrow 0$ it will approach the value of the molecule field detuning ε .

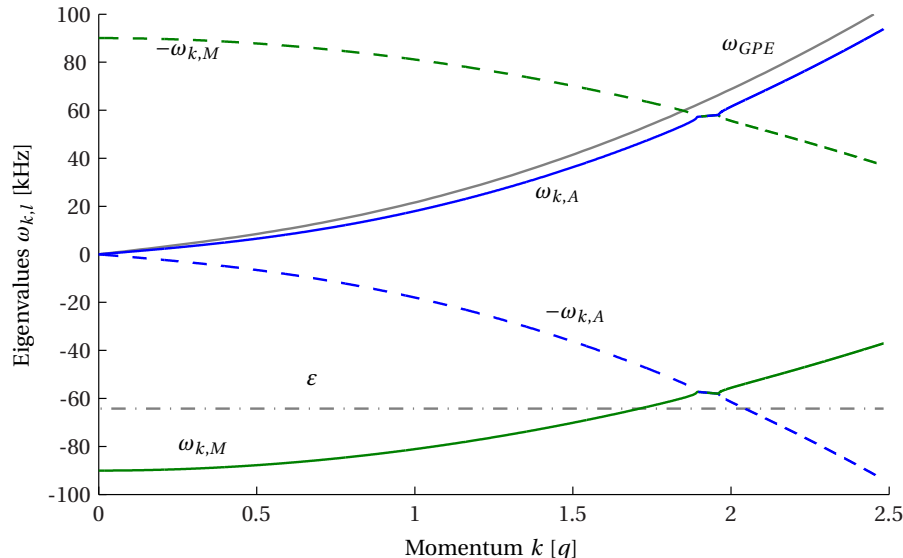


Figure 4: Eigenvalues $\omega_{k,A}$ (blue solid line) and $\omega_{k,M}$ (green solid line) as functions of the momentum k for ^{85}Rb at $900a_0$. The atom-dominated eigenvalue is similar to that obtained from the Gross-Pitaevskii equation (grey solid line), whereas the molecule-dominated eigenvalue is related to the molecule field detuning ε (grey dash-dotted line). The total density of the condensate is here 10^{20} m^{-3} and q is $1.6 \times 10^7 \text{ m}^{-1}$.

4.1.1 High momentum instability

As can be seen in Fig. 4, there is a crossover which occurs when $\omega_{k,A} + \omega_{k,M} = 0$, where the energy to create simultaneously a molecular-dominated quasiparticle and an atom-dominated quasiparticle is zero. As one proceeds through the crossover, the eigenvalue formula is determined successively by the procedures C, D and E, as given above. The midpoint of the crossover region is at the momentum

$$\frac{\hbar^2 k^2}{2m} = 2\mu_a - \frac{2}{3}(2U_{aa}n + \varepsilon). \quad (39)$$

Fig. 5 shows the behaviour of the high and low eigenvalues in the crossover region, where each eigenvalue has an imaginary part. The maximum amplitude of the imaginary parts of the eigenvalues is at approximately 1.5 kHz. For this system, we would therefore expect a relatively fast instability to occur — on a time scale of approximately 0.07 ms — with atom-molecule pairs being created and destroyed.

The instability arises because the energy to create a molecular quasiparticle of momentum \mathbf{k} becomes equal to the energy to destroy an atomic quasiparticle of momentum $-\mathbf{k}$. This is a natural instability to expect, and provides a mechanism for the condensate, which is metastable when the underlying interaction is attractive, to achieve its true ground state, a condensate of molecules. The relatively high value of the momentum required would make this a very much less important phenomenon in a trapped condensate, since the wavefunctions of high energy quasiparticles are largely located outside of the condensate. Since the transformation can only take place where there is a condensate, this would significantly decrease the size of the imaginary part.

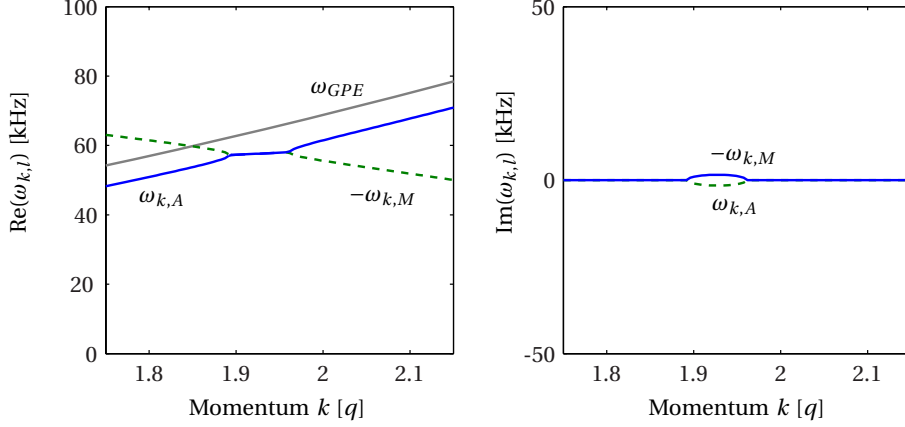


Figure 5: High eigenvalue (green dashed line) and low eigenvalue (solid blue line) for the same system as in figure 4 in the region where the energy associated with the destruction of an atom coincides with that of the creation of a molecule. The eigenvalues become complex where the overlap exists, with their real parts shown in the left panel and their respective imaginary components are shown in the right panel. As in figure 4, the grey line is the eigenvalue obtained from a system of structureless atoms.

4.2 Eigenvectors of the Bogoliubov-de Gennes equations

Using the normalisation condition (20) we can find a unique set of eigenvectors of the Bogoliubov-de Gennes equations corresponding to the eigenvalues (32–37):

$$u_{k,A} = \sqrt{\frac{1 - A_{k,M}^2(1 - C_{k,M}^2) - B_{k,M}^2}{(B_{k,A}^2 - A_{k,A}^2 C_{k,A}^2)(1 - A_{k,M}^2) - (B_{k,M}^2 - A_{k,M}^2 C_{k,M}^2)(1 - A_{k,A}^2)}}, \quad (40)$$

$$u_{k,M} = \sqrt{\frac{1 - (1 - A_{k,A}^2)u_{k,A}^2}{1 - A_{k,M}^2}}, \quad (41)$$

and, for $l = L, H$,

$$v_{k,A} = A_{k,A}u_{k,A}, \quad (42)$$

$$r_{k,A} = B_{k,A}u_{k,A}, \quad (43)$$

$$s_{k,A} = C_{k,A}v_{k,A}, \quad (44)$$

where

$$A_{k,A} = \frac{1}{\mathcal{M}_{11}} \left(-\mathcal{L}_{11} + \hbar\omega_{k,A} - \frac{\mathcal{L}_{12}^2}{\hbar\omega_{k,A} - \mathcal{L}_{22}} \right), \quad (45)$$

$$B_{k,A} = \frac{\mathcal{L}_{12}}{\hbar\omega_{k,A} - \mathcal{L}_{22}}, \quad (46)$$

$$C_{k,A} = -\frac{\mathcal{L}_{12}}{\hbar\omega_{k,A} + \mathcal{L}_{22}}. \quad (47)$$

The components of the eigenvectors for the same system as that in Fig. 4 are plotted in Fig. 6 as a function of the scattering length, for low momentum (Fig. 6(a)) and moderate momentum (Fig. 6(b)). At low scattering lengths, the eigenvector corresponding to the low eigenvalue $\omega_{k,A}$ is dominated by the atom components $u_{k,A}$ and $v_{k,A}$, with the

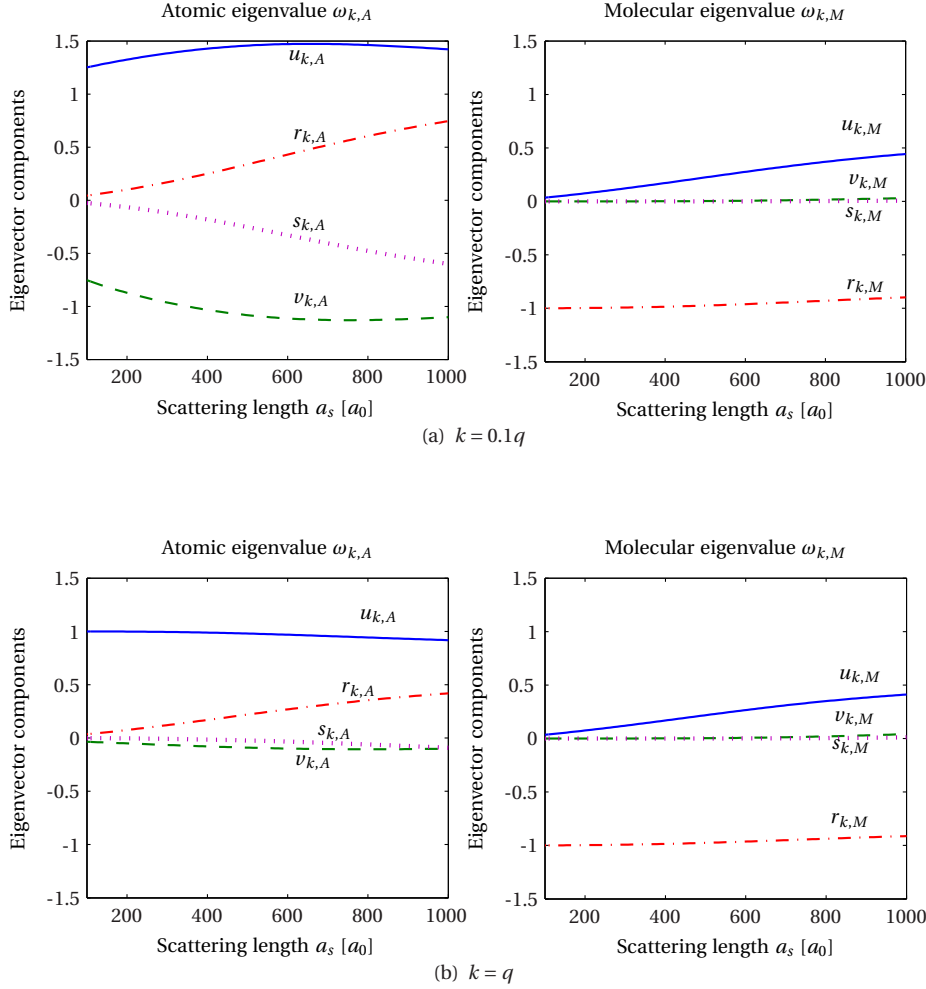


Figure 6: Eigenvector components $u_{k,A}$ (blue solid line), $v_{k,A}$ (green dashed line), $r_{k,A}$ (red dash-dotted line) and $s_{k,A}$ (cyan dotted line) for the low eigenvalue $\omega_{k,A}$ (left panel) and the high eigenvalue $\omega_{k,M}$ (right panel). The momentum is measured in units of the momentum q of the Bragg pulse in the experiment of Ref. [1] with $q = 1.6 \times 10^7 \text{ m}^{-1}$.

molecule components $r_{k,A}$ and $s_{k,A}$ becoming more significant the larger the scattering length. For larger scattering lengths, the amplitude of the molecule destruction operator is clearly significant compared to the atom one, and there is a large portion of molecules in the atom state.

For the higher eigenvalue $\omega_{k,M}$, the situation is reversed with the dominating eigenvector component being the one associated with the molecule destruction operator. Here we also see increased mixing between the two states as the scattering length is increased.

5 Application to Bragg scattering

The quasiparticle description of the excitations in our atom-molecule system can be used to describe the excitation spectrum from Bragg scattering. Following the procedure of [3] and [7], we derive the momentum transferred onto the condensate from an Bragg pulse, and compare the results we obtain here to those in [3].

The equations of motion for the coupled atom and molecule fields subject to a Bragg pulse are given by

$$i\hbar \frac{\partial \psi(\mathbf{x})}{\partial t} = \left(-\frac{\hbar^2 \nabla^2}{2m} + V_a(\mathbf{x}) \right) \psi(\mathbf{x}) + U_{aa} |\psi(\mathbf{x})|^2 \psi(\mathbf{x}) + \hbar V_{\text{opt}} \psi + g \psi(\mathbf{x})^* \phi(\mathbf{x}), \quad (48)$$

$$i\hbar \frac{\partial \phi(\mathbf{x})}{\partial t} = \left(-\frac{\hbar^2 \nabla^2}{4m} + \varepsilon + V_m(\mathbf{x}) \right) \phi(\mathbf{x}) + 2\hbar V_{\text{opt}} \cos(\mathbf{q} \cdot \mathbf{x} - \omega t) \phi + \frac{g}{2} \psi^2(\mathbf{x}), \quad (49)$$

where

$$V_{\text{opt}} = V_0(t) \cos(\mathbf{q} \cdot \mathbf{x} - \omega t), \quad (50)$$

where \mathbf{q} and ω are the wavevector and the frequency of the Bragg pulse respectively [3,8], and V_0 is the amplitude of the optical potential, given in terms of the Rabi frequency Ω and the excited state detuning Δ ,

$$V_0 = \frac{\hbar \Omega^2}{2\Delta}. \quad (51)$$

The optical potential for the molecule is chosen to be twice that of the atom on the assumption that the atoms in the molecule are very weakly bound, and for these purposes behave almost independently.

5.1 Quasiparticle evolution

Using the expansion (11), and the Bogoliubov-de Gennes equations, we can write the equations of motion

$$\mathbf{1} \sum_p \left(\mathbf{U}_p \dot{b}_p e^{-i\omega_p t} + \mathbf{V}_p^* \dot{b}_p^* e^{i\omega_p t} \right) = \mathcal{V}_{\text{opt}} \boldsymbol{\Psi}, \quad (52)$$

where

$$\mathcal{V}_{\text{opt}} = V_{\text{opt}} \begin{pmatrix} 1 & 0 \\ 0 & 2 \end{pmatrix}. \quad (53)$$

Similarly to the method in [9], we can project out b_p from the above equation by writing

$$\int d\mathbf{x} \left\{ \left(\mathbf{U}_{p'}^\dagger \mathcal{V}_{\text{opt}} \boldsymbol{\Psi} + \mathbf{V}_{p'}^\dagger \mathcal{V}_{\text{opt}} \boldsymbol{\Psi}^* \right) \right\} = \quad (54)$$

$$= \int d\mathbf{x} \sum_p \left\{ \mathbf{1} \mathbf{U}_{p'}^\dagger \left(\mathbf{U}_p \dot{b}_p e^{-i\omega_p t} + \mathbf{V}_p^* \dot{b}_p^* e^{i\omega_p t} \right) - \mathbf{1} \mathbf{V}_{p'}^\dagger \left(\mathbf{U}_p^* \dot{b}_p^* e^{i\omega_p t} + \mathbf{V}_p \dot{b}_p e^{-i\omega_p t} \right) \right\}, \quad (55)$$

$$= \mathbf{1} \sum_p \left\{ \int d\mathbf{x} \left(\mathbf{U}_{p'}^\dagger \mathbf{U}_p - \mathbf{V}_{p'}^\dagger \mathbf{V}_p \right) \dot{b}_p e^{-i\omega_p t} + \int d\mathbf{x} \left(\mathbf{U}_{p'}^\dagger \mathbf{V}_p^* - \mathbf{V}_{p'}^\dagger \mathbf{U}_p^* \right) \dot{b}_p^* e^{i\omega_p t} \right\}, \quad (56)$$

$$= \mathbf{1} \dot{b}_{p'}(t) e^{-i\omega_{p'} t}, \quad (57)$$

where on the last line we have used the normalisation and orthogonality conditions (16, 17). We therefore have

$$\dot{b}_p(t) = -\mathbf{1} e^{i\omega_p t} \int d\mathbf{x} \left\{ \left(\mathbf{U}_p^\dagger \mathcal{V}_{\text{opt}} \boldsymbol{\Psi} + \mathbf{V}_p^\dagger \mathcal{V}_{\text{opt}} \boldsymbol{\Psi}^* \right) \right\}, \quad (58)$$

Setting $\boldsymbol{\Psi} = (\psi_0, \phi_0)^T$, we get

$$b_p(t) = -\mathbf{1} \int_0^t e^{i\omega_p t'} dt' \int d\mathbf{x} \left\{ V_{\text{opt}} \left(\psi_0 (u_p^* + v_p^*) + 2\phi_0 (r_p^* + s_p^*) \right) \right\}. \quad (59)$$

Assuming that the Bragg pulse is square, with amplitude V_0 and duration T , we get

$$b_p(T) = -\frac{1V_0}{2} \int d\mathbf{x} \left(\psi_0(u_p^* + v_p^*) + 2\phi_0(r_p^* + s_p^*) \right) \times \int_0^T dt' e^{i\omega_p t'} \left(e^{i(\mathbf{q}\cdot\mathbf{x} - \omega t')} + e^{-i(\mathbf{q}\cdot\mathbf{x} - \omega t')} \right), \quad (60)$$

$$= -1V_0 e^{i\omega_p T/2} \int d\mathbf{x} \left(\psi_0(u_p^* + v_p^*) + 2\phi_0(r_p^* + s_p^*) \right) \times \left[e^{-i\omega T/2} e^{i\mathbf{q}\cdot\mathbf{x}} \frac{\sin((\omega_p - \omega)T/2)}{\omega_p - \omega} + e^{i\omega T/2} e^{-i\mathbf{q}\cdot\mathbf{x}} \frac{\sin((\omega_p + \omega)T/2)}{\omega_p + \omega} \right]. \quad (61)$$

5.2 Momentum transfer from uniform condensate

If considering the ideal case of Bragg scattering from a uniform condensate, the quasi-particle amplitudes are given by (40 – 44), and the ground state is given by (8, 9). The expression for b_p now simplifies to

$$b_p(T) = -\frac{1V_0}{\sqrt{V}} e^{i\omega_{k,A} T/2} \int_V d\mathbf{x} \left(\sqrt{n_a}(u_p^* + v_p^*) + 2\sqrt{n_m}(r_p^* + s_p^*) \right) e^{i\mathbf{k}\cdot\mathbf{x}} \times \left[e^{-i\omega T/2} \frac{\sin((\omega_p - \omega)T/2)}{\omega_p - \omega} e^{i\mathbf{q}\cdot\mathbf{x}} + e^{i\omega T/2} \frac{\sin((\omega_p + \omega)T/2)}{\omega_p + \omega} e^{-i\mathbf{q}\cdot\mathbf{x}} \right], \quad (62)$$

$$= -1V_0 \left(\sqrt{N_a}(u_p^* + v_p^*) + 2\sqrt{N_m}(r_p^* + s_p^*) \right) \times \left[e^{i(\omega_p - \omega)T/2} \frac{\sin((\omega_p - \omega)T/2)}{\omega_p - \omega} \delta_{p,-q} + e^{i(\omega_p + \omega)T/2} \frac{\sin((\omega_p + \omega)T/2)}{\omega_p + \omega} \delta_{p,q} \right], \quad (63)$$

where N_a and N_m are the number of atoms and molecules, respectively.

The total momentum imparted to the condensate can now be evaluated using the Bogoliubov expansions (11), and the normalisation and orthogonality relations (16, 17, 20),

$$P(T) = \frac{\hbar}{2i} \int d\mathbf{x} \left\{ \psi^* \nabla \psi + \frac{1}{2} \phi^* \nabla \phi \right\} + \text{c.c.} \\ = \sum_p \hbar p \left(|b_p(T)|^2 + \frac{1}{2} |b_p(T)|^2 \right) \\ = \frac{3\hbar q V_0^2}{2} \sum_l \left[\left(\frac{\sin((\omega_{q,l} - \omega)T/2)}{\omega_{q,l} - \omega} \right)^2 - \left(\frac{\sin((\omega_{q,l} + \omega)T/2)}{\omega_{q,l} + \omega} \right)^2 \right] \\ \times \left| \sqrt{N_a}(u_q + v_q) + 2\sqrt{N_m}(r_q + s_q) \right|^2. \quad (64)$$

It is clear that this expression will have its maximum values at the points where $\omega = \omega_{q,l}$, and if the atom field is much larger than the molecular field — as is the case for the system studied here — the only significant maximum will be at the lower eigenvalue ω_L . Consequently the Bragg resonance peak will occur at the eigenvalue of the atom state, $\omega_{k,A}$ in figure 4, corresponding to the momentum of the Bragg pulse.

Fig. 7 shows the fraction of particles being scattered out of the condensate during the Bragg pulse for three different scattering lengths. The portion of scattered particles is related to the momentum transfer as $P/\hbar q N$, where $N \equiv N_a + 2N_m$ is the total number of particles. The resonance peak of the Bragg spectrum shifts to higher frequencies as the scattering length is increased. However, this shift starts to decrease when the scattering

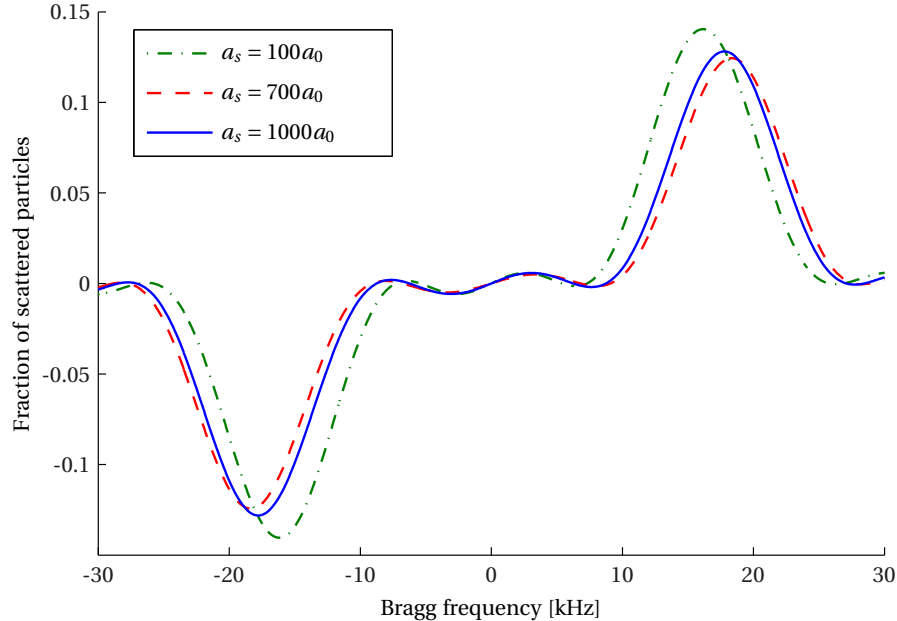


Figure 7: Bragg spectrum showing the fraction of particles scattered out of the condensate as a function of the Bragg frequency for a uniform system ^{85}Rb with total density of 10^{20} m^{-3} . Here we show the spectra for three different scattering lengths: $a_s = 100a_0$ (green dashed-dotted line), $a_s = 700a_0$ (red dashed line) and $a_s = 1000a_0$ (blue solid line). The duration of the Bragg pulse is $T = 0.1\text{ms}$, and the intensity of the pulse is $V_0 = 2\pi \times 1 \text{ kHz}$.

length is larger than approximately $700a_0$. The free particle resonance is located at $1/2\pi \times \hbar q^2/2m \approx 15.4 \text{ kHz}$.

Fig.8 shows how the shift of the Bragg resonance from the free particle resonance changes with the increase in the scattering length. For comparison we have also plotted the result based on the model of a condensate of structureless atoms with increased scattering length [3]. The two models agree well for low scattering lengths, but differ dramatically for larger scattering lengths. In the figure we have also marked the scattering lengths for which there is available data of the binding energy, as in [5]. The values outside of these are calculated by the method described in Section 2.

6 Conclusion

The Bragg peak shift obtained from our model of a coupled atom-molecule condensate is significantly different from that obtained by a model of structureless atoms. Even though it describes the ideal case of Bragg scattering from a uniform condensate and is therefore not directly comparable to that obtained in the experiment of Ref. [1], it is still qualitatively similar to this. Most importantly, unlike other approaches to this problem, for example that by Kinnunen *et al* [10], the lineshift in figure 8 shows a clear *downward* behaviour for large scattering lengths, exactly as was reported experimentally in [1].

In *Paper III* we will implement the formalism described here and in *Paper I* in full numerical calculations of Bragg scattering from an inhomogeneous BEC. The results from these simulations will be directly comparable to the results from the experiment of [1].

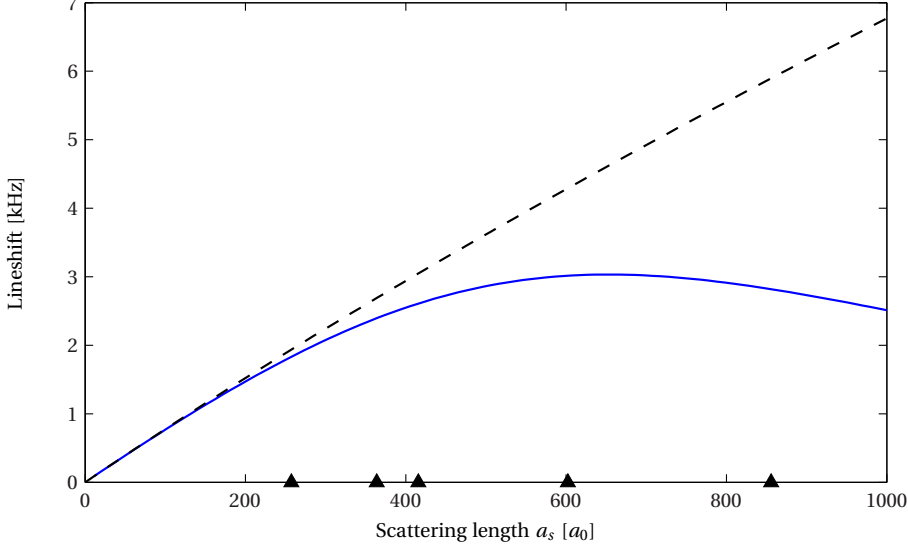


Figure 8: The shift of the peak of the Bragg spectra from that of the non-interacting gas, plotted against the scattering length a_s . The solid blue line is based on the peak position calculated by (64), and the black dashed line is the equivalent calculation based on the model of structureless atoms, as in [3]. The black triangles mark the values of the scattering length for which Ref. [5] gives experimental data of the binding energy.

A Orthogonality and normalization conditions

The orthogonality conditions of the quasiparticle amplitudes can be derived by writing

$$\hbar\omega_p \int d\mathbf{x} (\mathbf{U}_{p'}^\dagger \mathbf{U}_p - \mathbf{V}_{p'}^\dagger \mathbf{V}_p) = \int d\mathbf{x} \mathbf{U}_{p'}^\dagger (\mathcal{L} \mathbf{U}_p + \mathcal{M} \mathbf{V}_p) + \int d\mathbf{x} \mathbf{V}_{p'}^\dagger (\mathcal{L} \mathbf{V}_p + \mathcal{M}^\dagger \mathbf{U}_p) \quad (65)$$

$$\hbar\omega_{p'} \int d\mathbf{x} (\mathbf{U}_{p'}^\dagger \mathbf{U}_p - \mathbf{V}_{p'}^\dagger \mathbf{V}_p) = \int d\mathbf{x} (\mathbf{U}_{p'}^\dagger \mathcal{L} + \mathbf{V}_{p'}^\dagger \mathcal{M}^\dagger) \mathbf{U}_p + \int d\mathbf{x} (\mathbf{V}_{p'}^\dagger \mathcal{L}^\dagger + \mathbf{U}_{p'}^\dagger \mathcal{M}) \mathbf{V}_p. \quad (66)$$

The Hermitian nature of \mathcal{L} means that the two right hand sides are equal so that, for an appropriate normalization we can write

$$\int d\mathbf{x} (\mathbf{U}_{p'}^\dagger \mathbf{U}_p - \mathbf{V}_{p'}^\dagger \mathbf{V}_p) = \delta_{p,p'}. \quad (67)$$

Since both \mathcal{L} and \mathcal{M} are symmetric we can then write

$$\hbar\omega_{p'} \int d\mathbf{x} (\mathbf{V}_p^T \mathbf{U}_{p'} - \mathbf{U}_p^T \mathbf{V}_{p'}) = \int d\mathbf{x} \{ \mathbf{V}_p^T (\mathcal{L} \mathbf{U}_{p'} + \mathcal{M} \mathbf{V}_{p'}) + \mathbf{U}_p^T (\mathcal{L} \mathbf{V}_{p'} + \mathcal{M}^\dagger \mathbf{U}_{p'}) \} \quad (68)$$

$$\hbar\omega_p \int d\mathbf{x} (\mathbf{V}_p^T \mathbf{U}_{p'} - \mathbf{U}_p^T \mathbf{V}_{p'}) = - \int d\mathbf{x} \{ (\mathbf{V}_p^T \mathcal{L} + \mathbf{U}_p^T \mathcal{M}^*) \mathbf{U}_{p'} - (\mathbf{U}_p^T \mathcal{L} + \mathbf{V}_p^T \mathcal{M}) \mathbf{V}_{p'} \}, \quad (69)$$

so that, assuming $\omega_p \neq -\omega_{p'}$, we can say

$$\int d\mathbf{x} (\mathbf{V}_p^T \mathbf{U}_{p'} - \mathbf{U}_p^T \mathbf{V}_{p'}) = 0. \quad (70)$$

We can also find normalisation conditions using the Bose commutation relations for the components of $\boldsymbol{\psi} = (\psi, \phi)^T$,

$$\begin{aligned}\delta_{\alpha,\beta}\delta(\mathbf{x}-\mathbf{x}') &= [\boldsymbol{\psi}_\alpha(\mathbf{x}), \boldsymbol{\psi}_\beta^\dagger(\mathbf{x}')] & (71) \\ &= \sum_{p,p'} \left\{ \mathbf{U}_{\alpha,p}(\mathbf{x}) \mathbf{U}_{\beta,p'}^*(\mathbf{x}') [\hat{b}_p(\mathbf{x}), \hat{b}_{p'}^\dagger(\mathbf{x}')] + \mathbf{V}_{\alpha,p}^*(\mathbf{x}) \mathbf{V}_{\beta,p'}(\mathbf{x}') [\hat{b}_p^\dagger(\mathbf{x}), \hat{b}_{p'}(\mathbf{x}')] \right. \\ &\quad \left. + \mathbf{U}_{\alpha,p}(\mathbf{x}) \mathbf{V}_{\beta,p'}(\mathbf{x}') [\hat{b}_p(\mathbf{x}), \hat{b}_{p'}(\mathbf{x}')] + \mathbf{V}_{\alpha,p}^*(\mathbf{x}) \mathbf{U}_{\beta,p'}^*(\mathbf{x}') [\hat{b}_p^\dagger(\mathbf{x}), \hat{b}_{p'}^\dagger(\mathbf{x}')] \right\} & (72)\end{aligned}$$

from which, assuming that the quasiparticle operators \hat{b}_p obey the usual Bose commutation relations, we get the normalisation condition of the amplitudes,

$$\sum_p (\mathbf{U}_{\alpha,p} \mathbf{U}_{\beta,p}^* - \mathbf{V}_{\alpha,p}^* \mathbf{V}_{\beta,p}) = \delta_{\alpha,\beta} \quad (73)$$

Similarly, the other commutation relation,

$$\begin{aligned}0 &= [\boldsymbol{\psi}_\alpha(\mathbf{x}), \boldsymbol{\psi}_\beta(\mathbf{x}')] & (74) \\ &= \sum_{p,p'} \left\{ \mathbf{U}_{\alpha,p}(\mathbf{x}) \mathbf{U}_{\beta,p'}(\mathbf{x}') [\hat{b}_p(\mathbf{x}), \hat{b}_{p'}(\mathbf{x}')] + \mathbf{V}_{\alpha,p}^*(\mathbf{x}) \mathbf{V}_{\beta,p'}^*(\mathbf{x}') [\hat{b}_p^\dagger(\mathbf{x}), \hat{b}_{p'}^\dagger(\mathbf{x}')] \right. \\ &\quad \left. + \mathbf{U}_{\alpha,p}(\mathbf{x}) \mathbf{V}_{\beta,p'}^*(\mathbf{x}') [\hat{b}_p(\mathbf{x}), \hat{b}_{p'}^\dagger(\mathbf{x}')] + \mathbf{V}_{\alpha,p}^*(\mathbf{x}) \mathbf{U}_{\beta,p'}(\mathbf{x}') [\hat{b}_p^\dagger(\mathbf{x}), \hat{b}_{p'}(\mathbf{x}')] \right\} & (75)\end{aligned}$$

gives the condition

$$\sum_p (\mathbf{U}_{\alpha,p} \mathbf{V}_{\beta,p}^* - \mathbf{V}_{\alpha,p}^* \mathbf{U}_{\beta,p}) = 0. \quad (76)$$

References

- [1] S. B. Papp, J. M. Pino, R. J. Wild, S. Ronen, C. E. Wieman, D. S. Jin, and E. A. Cornell. Bragg Spectroscopy of a Strongly Interacting ^{85}Rb Bose-Einstein Condensate. *Phys. Rev. Lett.*, 101(13):135301, Sep 2008.
- [2] C. E. Sahlberg and C. W. Gardiner. Effective field theory for atom-molecule systems I: Formulation of effective field theory, 2010.
- [3] P. B. Blakie, R. J. Ballagh, and C. W. Gardiner. Theory of coherent Bragg spectroscopy of a trapped Bose-Einstein condensate. *Phys. Rev. A*, 65:033602, 2002.
- [4] P. B. Blakie, A. S. Bradley, M. J. Davis, R. J. Ballagh, and C. W. Gardiner. Dynamics and statistical mechanics of ultra-cold Bose gases using c-field techniques. *Advances in Physics*, 57:363–455, September 2008.
- [5] N. R. Claussen, S. J. J. M. F. Kokkelmans, S. T. Thompson, E. Donley, E. Hodby, and C. E. Weiman. Very-high-precision bound-state spectroscopy near a ^{85}Rb Feshbach resonance. *Phys. Rev. A*, 67(0):069791(R), 2003.
- [6] E. Braaten and H.-W. Hammer. Feshbach Resonances in Ultracold Gases. *Phys. Rep.*, 00(428):259–390, 2006.
- [7] C. Tozzo and F. Dalfovo. Bogoliubov spectrum and Bragg spectroscopy of elongated Bose-Einstein condensates. *New Journal of Physics*, 5(1):54, 2003.
- [8] P. B. Blakie and R. J. Ballagh. Mean-field treatment of Bragg scattering from a Bose-Einstein condensate. *J. Phys. B: At. Mol. Opt. Phys.*, 33:3961–3982, 2000.

- [9] S. A. Morgan, S Choi, K. Burnett, and M. Edwards. Nonlinear mixing of quasiparticles in an inhomogeneous Bose condensate. *Phys. Rev. A*, 57(5):3818, 1998.
- [10] J J Kinnunen and M J Holland. Bragg spectroscopy of a strongly interacting Bose-Einstein condensate. *New J. Phys.*, 11:013030, 2009.